Inorganic Chemistry

pubs.acs.org/IC Article

Electronic Structural Studies of the Ru₃(III,II,II) Mixed-Valent State of Oxo-Centered Triruthenium Clusters

Joseph M. Palasz, Tyler M. Porter, and Clifford P. Kubiak*



Cite This: Inorg. Chem. 2020, 59, 10532–10539



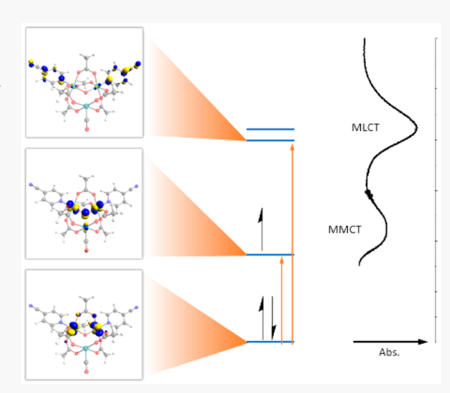
ACCESS

Metrics & More

Article Recommendations

Supporting Information

ABSTRACT: The anionic state of basic ruthenium acetate complexes of the type $[Ru_3O(OAc)_6](CO)(L_1)(L_2)$ (L=4-cyanopyridine, pyridine, and N,N-dimethylaminopyridine) feature pronounced optical transitions in the near-infrared region indicative of strongly coupled mixed-valence states. A series of these clusters was prepared and studied spectroscopically in tandem with density functional theory (DFT) computational results to construct an orbital structure—function description of how the electron density is shared between the ruthenium centers in this mixed-valent state. The mixed-valency manifests itself as a combination of the nonbonding atomic orbitals of the equivalent ruthenium centers, with increased energetic splitting between the orbitals with symmetries appropriate for more efficient electronic communication. This DFT-based model agrees with the Marcus—Hush description of mixed-valency, with the added knowledge that specific orbitals contribute to different degrees in the electronic coupling between two redox centers.



■ INTRODUCTION

Mixed-valence compounds are molecular donor-bridgeacceptor systems within which intramolecular electron transfer (ET) can occur between the donor and acceptor. The first inorganic molecular mixed-valence complex was reported over 40 years ago by Creutz and Taube. Since then, the field has expanded significantly as inorganic mixed-valency has been found to play vital roles in the function of various metalloproteins (e.g., oxygen evolution complex, cytochrome c oxidase, nitric oxide reductase, and ribonucleotide reductase)²⁻⁷ as well as in various synthetic applications (molecular magnets and conductive materials). 8-13 The redox states of the metal centers in mixed-valent complexes can be localized or delocalized to varying degrees, and the Robin-Day classification was introduced early on to distinguish between systems that are completely localized (class I), delocalized (class III), or in between (class II).14 Hush introduced a theoretical framework for explaining how the extent of electron delocalization manifests in the intervalence charge transfer (IVCT) bands of the electronic absorption spectra, invoking a simple exchange operator to couple charge states of the equivalent redox centers. 15 While these types of descriptions have proven invaluable in modeling the behavior of mixedvalent systems, they fall short of providing an explanation for the origins of electronic delocalization within a molecular structure.

To successfully develop electronic structure—function relationships for inorganic mixed-valent compounds it requires an intricate description of these molecules, accounting for relationships between the metal orbitals, ligand geometry, and molecular surroundings. To this end, experimentalists have

sought the assistance of computational methods like density functional theory (DFT) to surpass what pen and paper descriptions can possibly provide. Inherently the paramagnetic and delocalized nature of mixed-valent species makes calculations on these species challenging, especially when heavy metals are included in the structure. However, with the increasing capability of hardware to tackle expensive calculations and with impressive method development toward tuning degrees of electronic delocalization, 16-22 DFT has started to provide meaningful and unique insight into the behavior of inorganic mixed-valent molecules. 19,23

Herein, we examined a series of oxo-centered triruthenium acetate clusters $(Ru_3(\mu_3\text{-O})(OAc)_6(CO)(L_1)(L_2))$ to gain a better understanding of the electronic structure of highly delocalized mixed-valent systems (Figure 1). By employing the strengths provided from synthesis by creating a series of molecules varying by Hammett substituents, and using computation to construct detailed orbital pictures of the molecules, we hope to build an understanding of how nuanced changes in the ligand character can alter the observed absorption spectra of these molecules.

The appeal of these molecules lies in their ease of synthesis, modular nature via substitution of the ancillary pyridine

Received: March 24, 2020 Published: July 16, 2020





Ligand Abbreviations

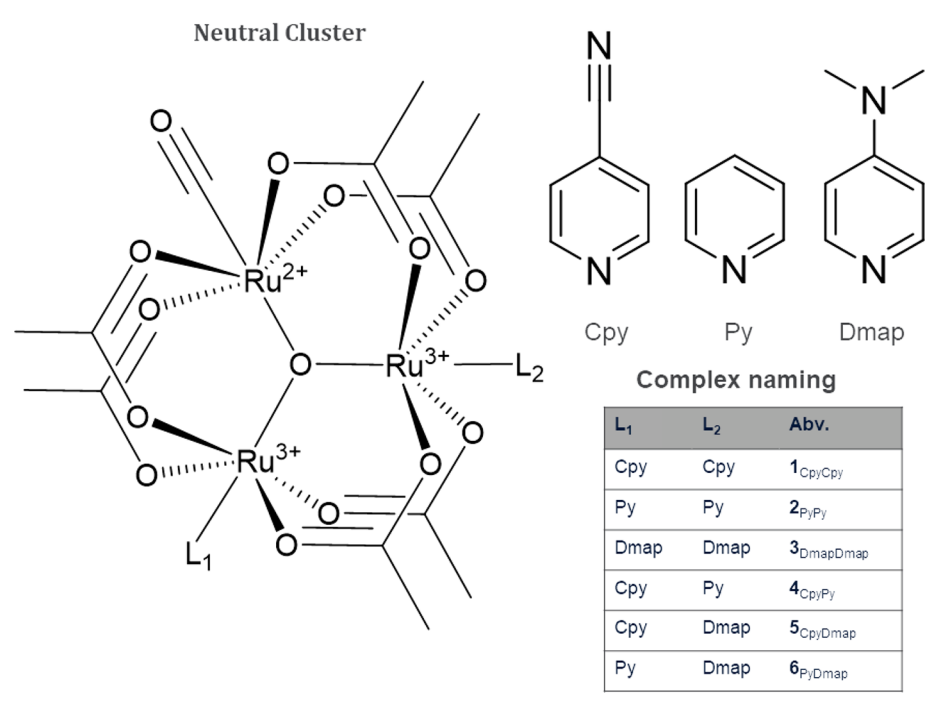


Figure 1. Structure of the neutral forms of the oxo-centered triruthenium acetate clusters studied in this paper, with abbreviations listed for the ancillary ligands.

ligands, and redox-stability of their mixed-valent anionic state. This has resulted in a substantial body of literature describing their behavior. 24-34 These complexes consist of three ruthenium centers in a trigonal planar geometry surrounding a μ_3 -bridging oxygen and straddled by six bridging acetates. Each ruthenium center is in a pseudo-octahedral geometry, capped by a single ancillary ligand trans to the μ_3 -oxo ligand.³⁵ The two Ru(III) centers are capped by sterically unhindered pyridine ligands, while the Ru(II) site is capped by a carbonyl. The introduction of the carbonyl ligand provides a convenient spectroscopic handle, while the structural integrity of the metal-carboxylate core provides well-behaved, reversible electrochemistry when measured by cyclic voltammetry. 36-39 Upon a one-electron reduction (Ru₃(III,III,II) → Ru₃(III,II,II)), the anionic triruthenium clusters, [1_{CpyCpy}]⁻-[6_{PyDmap}] (Cpy, 4-cyanopyridine; Py, pyridine; Dmap, N,Ndimethyl-4-aminopyridine), display an intense absorbance (ε > 4000 M^{-1} cm⁻¹) in the near-infrared (NIR) region, which appeared to be multiple overlapping features. An intense NIR absorbance is characteristic behavior indicative of a strongly coupled mixed-valent system. 40-42 The mixed-valent character in this state originates from an electronic coupling between Ru(II) and Ru(III) states of the two pyridine-ligated ruthenium atoms. While it has not yet been possible to characterize the Ru₃(III,II,II) state by X-ray crystallography, from the proximity of the ruthenium atoms, we expect a significantly delocalized electron density between the two ruthenium centers. The presence of a complex NIR absorption spectrum suggests a more nuanced interaction than what would be expected in a traditional two-state model, which anticipates a single Gaussian feature as a result of the two states. Within this study, we describe the NIR electronic absorption spectra and our description of the mixed valency

within the framework of DFT results for this series of complexes.

EXPERIMENTAL AND COMPUTATIONAL METHODS

All chemicals and solvents were used as-received unless otherwise noted. Complexes 1-6 were synthesized according to literature procedures and stored at room temperature under nitrogen in a glovebox.⁴³ bis(pentamethylcyclopentadienyl)cobalt(II) ((Cp*)₂Co-(II)) was used as-received from Sigma-Aldrich and stored in a glovebox freezer at -34 °C. All solvents were dried over an alumina column under an argon atmosphere on a Grubbs-style solvent purification system.

Reduction of Neutral Compounds 1–6. Stock solutions of the neutral molecules $\mathbf{1}_{\mathrm{CpyCpy}}$ – $\mathbf{6}_{\mathrm{PyDmap}}$ at concentrations ranging from 3 to 10 mM were prepared under a nitrogen atmosphere using degassed acetonitrile (MeCN) stored over 3 Å molecular sieves. The stock solution for each molecule was used to prepare six solutions with concentrations ranging from 0.5–3 mM. A solution of $(\mathrm{Cp}^*)_2\mathrm{Co}(\mathrm{II})$ in dry MeCN was added in stoichiometric quantities to each aliquot affording the singly reduced anions $[\mathbf{1}_{\mathrm{CpyCpy}}]^- - [\mathbf{6}_{\mathrm{PyDmap}}]^-$ at six equally spaced concentrations between 0.2 and 2 mM. The progress of the reduction was monitored by FTIR spectroscopy where the disappearance of the $\nu(\mathrm{CO})$ band for the neutral cluster $(\nu(\mathrm{CO}) \approx 1940~\mathrm{cm}^{-1})$ and the appearance of a red-shifted $\nu(\mathrm{CO})$ band near $1900~\mathrm{cm}^{-1}$ indicative of the anionic cluster were observed.

UV–Vis Data Collection and Analysis. UV–vis spectra were collected on a Shimadzu UV-3600 UV–vis/NIR spectrometer. Immediately following the reduction of complexes $\mathbf{1}_{\mathsf{CpyCpy}} - \mathbf{6}_{\mathsf{PyDmap}}$ under a N_2 atmosphere, the solutions were placed in an airtight Suprasil quartz cuvette with a path length of 1 mm, and the electronic absorption spectrum was collected across 300–1600 nm. Molar extinction coefficients (ε) were determined by linear regression of the absorption maximum for the measured spectra of $[\mathbf{1}_{\mathsf{CpyCpy}}]^- - [\mathbf{6}_{\mathsf{PyDmap}}]^-$ at six known concentrations. Spectral deconvolutions were done in OriginPro 8.5 by fitting the NIR peaks as two Gaussian

Table 1. Electronic Characterization of the Anions of 1-6^a

		absorbance maximum, cm $^{-1}$ (ε , M $^{-1}$ ·cm $^{-1}$)			
	first reduction potential (V vs Fc)				
$[1_{CpyCpy}]^-$	-1.14	7986 (2472) ^b	9439 (7125) ^b	17094 (15314)	
$[2_{\mathrm{PyPy}}]^-$	-1.36	$8209 (2635)^{b}$	9374 (3471) ^b	21008 (16854)	
$[3_{\mathrm{DmapDmap}}]^{-}$	-1.56	$8278 (3395)^{b}$	9435 (2921) ^b	24509 (11152)	
$[4_{\mathrm{CpyPy}}]^{-}$	-1.22	$8289 (2479)^b$	$10023 (6453)^b$	16666 (12173)	22421 (4772)
$[5_{CpyDmap}]^-$	-1.30	8671 (949) ^b	$10418 (3235)^{b}$	16556 (6132)	
$[6_{ m PyDmap}]^-$	-1.44	8341 (3145) ^b	9651 (3200) ^b	20661 (8053)	

^aTabulated first reduction potentials of the neutral molecules 1–6 corresponding to the relative stabilities of the anions studied in this paper. (First column) Absorption features and attenuation coefficients observed in the UV–vis/NIR spectrum (Second column). ^bAbsorbance maxima and molar attenuation coefficient for overlapping peaks determined from a peak fitting algorithm in OriginPro version 8.5.

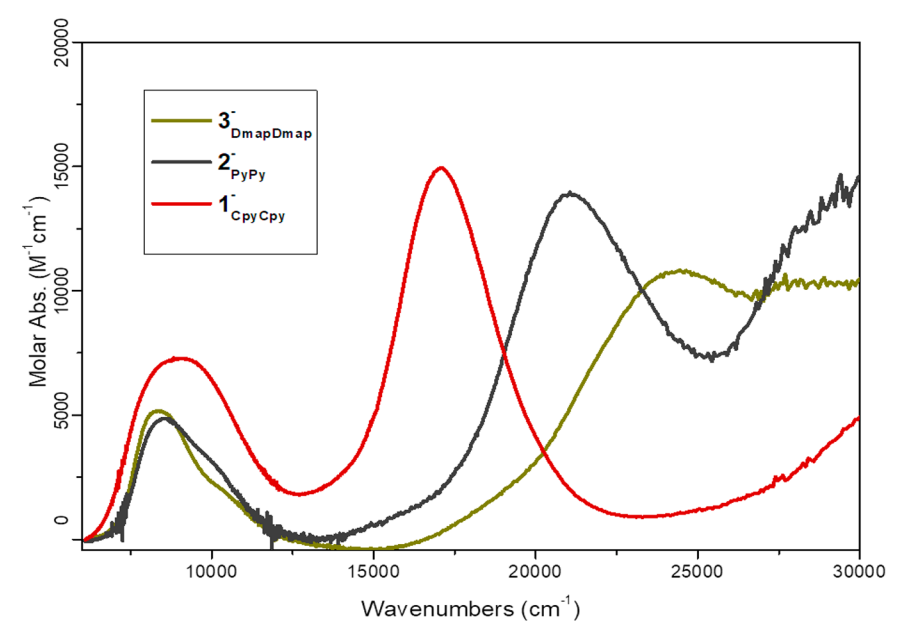


Figure 2. Visible/NIR absorption spectra of the reduced state of molecules $[1_{CpyCpy}]^-$, $[2_{pyPy}]^-$, and $[3_{DmapDmap}]^-$ in acetonitrile.

features and the metal-to-ligand charge-transfer (MLCT) as a single Voiet line shape.

Electrochemical Measurements. Cyclic voltammetry was performed on a BASi Epsilon potentiostat in dry MeCN degassed under argon with 0.1 M tetrabutylammonium hexafluorophosphate (TBAPF₆, recrystallized from anhydrous EtOH and vacuum-dried at 80 °C) as the supporting electrolyte. The first reduction feature observed for each cluster is listed in Table 1.

Density Functional Theory. Calculations were performed in the ORCA software suite (version 4.0.1.2) at the B3LYP/G level of theory with the RIJCOSX approximation. Geometry optimizations were performed starting from XYZ coordinates adapted from the reported crystal structure of a neutral Ru₃O cluster.²⁸ All atoms were treated with the def2-TZVP basis set for the geometry optimizations, while the single-point energy used the def2-QZVP basis set for ruthenium atoms and def2-TZVP for all other atoms. Both sets of calculations employed the def2/J auxiliary basis sets. 44-47 Dispersion corrections were applied with the Becke-Johnson damping scheme (D3BJ), and solvation was accounted for by using the CPCM solvation model in MeCN. 48,49 Displayed orbital energies are taken as the calculated quasi-restricted molecular orbitals for complete occupancy and as an average of the α and β spin orbitals for partially occupied orbitals. When displayed versus the ferrocene/ferrocenium redox potential (Fc+/0), the orbital energies were normalized to make the first reduction potential of the cluster equivalent to the energy of the singly occupied molecular orbital (SOMO).

■ RESULTS AND DISCUSSION

Absorption Spectra of Reduced Clusters. The UV-vis/ NIR absorption spectra for the series of reduced clusters feature two prominent absorptions within the region of 300-1600 nm. In the visible region of the spectra, all clusters display a single intense feature that changes energy with pyridine ligand substitution. In the symmetric clusters [1_{CpyCpy}]-, $[2_{p_yp_y}]^-$, and $[3_{DmapDmap}]^-$ this absorption maximum shifts to higher energy as the pyridine ligands become more electrondonating (Figure 2). This transition is experimentally assigned as a metal-to-ligand charge-transfer (MLCT) from the metal centered highest occupied molecular orbital (HOMO) to the ligand-based lowest unoccupied molecular orbital (LUMO). This is further supported across the series of molecules $[1_{CpyCpy}]^-$, $[4_{CpyPy}]^{-1}$ and $[5_{CpyDmap}]^-$ in which this feature stays roughly at the same energy as the Cpy ligand is maintained. In $[4_{CpyPy}]^-$, the weak high energy transition centered at 22421 cm⁻¹ may arise from MLCT to the more electron rich pyridine substituent with a higher energy π^* orbital. However, in $[5_{CpyDmap}]^-$ and $[6_{PyDmap}]^-$ this feature is not completely resolvable as overlap with other strong absorbances preclude a definitive assignment.

It is well documented that the presence of a NIR absorption feature can be the result of two electronically coupled states within a mixed-valent molecule. 40 The intense and broad

absorption in the NIR region (7000–12000 cm^{-1}) for $1^--6^$ can be reasonably fit by two Gaussian functions (S13-S15), indicating a more complicated mixed-valence interaction than a typical two-state description, possibly indicating either a mediating third state⁵⁰ or distinct electronic couplings between different metal-centered orbitals. Either explanation obfuscates any conclusive attempt to describe these systems with a singular coupling term (H_{ab}). This assignment as a metal-tometal charge-transfer (MMCT) is well represented in complex 3⁻ by the steep intensity loss on the low energy side of the NIR band, resulting in a deviation from the Gaussian fit. The "clipping" of the intensity on the low energy of an IVCT band is generally explained to result from the flattening of the potential energy surface as a mixed-valence system moves through the Robin-Day Class II/III borderline. 15,40,50 While the peak energies of the homoleptic clusters (1^--3^-) do not change significantly with ligand substitution, the NIR bands along the series of clusters $[1_{CpvCpv}]^-$, $[4_{CpvPv}]^-$, and [5_{CpyDmap}] blue shift with increasing electronic asymmetry, as demonstrated in Figure 3. That is, as the difference in donor

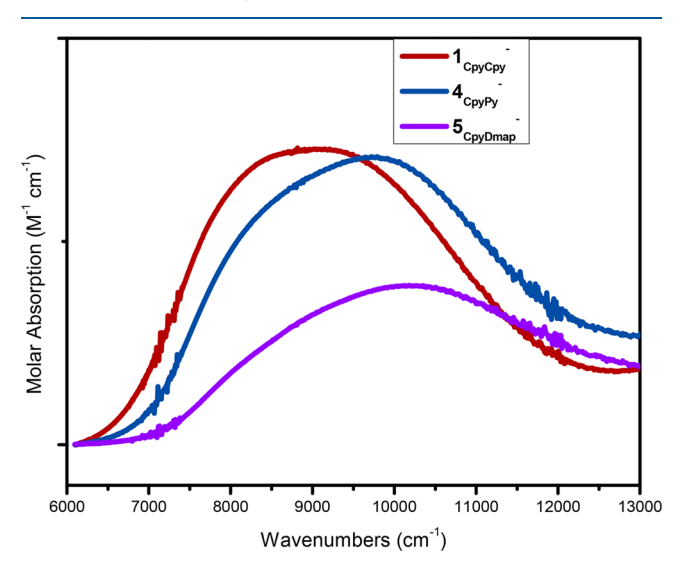


Figure 3. NIR region of clusters containing 4-cyanopyridine as a ligand, demonstrating the blue shifting and loss of intensity of the feature as the electronic mismatch between pyridine-type ligands increases.

strength between L_1 and L_2 increases, a larger blue shift of the NIR band is observed. Upon spectral deconvolution, complexes $[\mathbf{2}_{PyPy}]^-$ and $[\mathbf{3}_{DmapDmap}]^-$ display a large decrease in intensity for the higher energy feature with respect to $[\mathbf{1}_{CpyCpy}]^-$ with minimal changes in energy (400 cm $^{-1}$ >). The series of molecules containing Dmap as a ligand, $[\mathbf{3}_{DmapDmap}]^-$, $[\mathbf{6}_{DmapPy}]^-$, and $[\mathbf{5}_{DmapCpy}]^-$, demonstrate both trends simultaneously, showing a blue shift with increasing ligand mismatch and a decrease in the intensity of the high-energy feature with the more electron-rich ligands.

Density Functional Theory Results. The outputs from the DFT calculations show that the electronic structures of the anions $[1_{CpyCpy}]^--[6_{PyDmap}]^-$ are homologous across the series. Modest changes in the orbital composition and energy levels are observed with pyridine ligand substitution. For simplicity, the orbital iso-surfaces of the frontier orbitals for $[1_{CpyCpy}]^-$ are shown in Figure 4 and are representative of the entire series. The CO-ligated ruthenium center (Ru_{CO}) is significantly affected by the distinct coordination environment,

as π -backbonding to the CO substantially stabilizes the nonbonding d orbitals compared to the pyridine-ligated ruthenium atoms (Ru_L). The six highest energy populated orbitals in all clusters are dominated by the nonbonding d orbitals of the two Ru_L centers. In the symmetric anions $[1_{\text{CpyCpy}}]^-$, $[2_{\text{PyPy}}]^-$, and $[3_{\text{DmapDmap}}]^-$, these are linear combinations of the Ru_L d orbitals, with some contribution from the bridging oxide ligand. The three symmetric combinations of d orbitals are lower in energy than the three antisymmetric combinations.

For each Ru_L, the z-axis can be defined along the Ru-L bond and the y-axis as normal to the plane containing the three ruthenium centers; the SOMO is a π system formed from the participation of the d_{vz} orbitals for both Ru_L's with the p orbital of the bridging oxide ligand. The HOMO is then a combination of the dxv orbitals from both RuL's and the HOMO-1 is a combination of the d_{xz} orbitals. This ranking of energy levels for these frontier orbitals can be qualitatively rationalized as the electron density from the π -system of the cluster destabilizing the d orbitals sharing that symmetry, with the d_{xz} orbitals being the least affected by that density, as they are within the plane of the molecule. Across the anions $[1_{CpyCpy}]^-$, $[2_{PyPy}]^-$, and $[3_{DmapDmap}]^-$, as more electrondonating pyridine ligands are used, a divergence of the SOMOs and HOMOs from the lower lying d orbitals is observed. This implies that the electron-withdrawing pyridine ligands stabilize the π -system and reduce the energetic splitting between the orbitals. The LUMO for all clusters is primarily centered on the pyridine ligand π^* orbital. In the asymmetrically substituted anions, the LUMO is localized on the most electron-withdrawing pyridine, while the LUMO+1 is based on the more electron-donating ligand.

In $[4_{CpyPy}]^--[6_{PyDmap}]^-$, the asymmetry perturbs the orbitals, resulting in a greater localized electron density on a single ruthenium center, which is most clearly seen in Figure 5. The energetic ordering and spatial orientation of these orbitals are identical to the homoleptic clusters; however, the charge density of the orbitals is shifted, reflecting a localization of charge on the more electron-deficient ruthenium center.

The tentative assignments of the observed transitions in the electronic absorption spectra are consistent with the computed frontier orbitals. B3LYP is generally known to overestimate electronic delocalization, which should result in some exaggeration of the energy splitting due to the coupling between states. However, for $[1_{CpyCpy}]^-$, the calculated energy gaps between the HOMO and LUMO correspond well with the observed absorption peak energy ($\Delta E < 1000 \text{ cm}^{-1}$) and matches with the qualitative description of the feature as a MLCT. This assignment is further supported by the increase in this energy for $[2_{PyPy}]^-$ and $[3_{DmapDmap}]^-$. While the calculated energy of the LUMO is typically suspect at this level of calculation, the similarity in the behavior of the HOMO-LUMO energy differences and the observed absorbance features provide confidence that the DFT calculation is adequately capturing the electronic structure of the molecules. As more electron-donating ligands are used in $[2_{P_VP_V}]^-$ and $[3_{DmapDmap}]^{-}$, a slight discrepancy between the blue-shift for the orbital spacings and experimental absorbances arises (Figure 6). This is expected, as the degree of delocalization within these clusters is highly dependent on the ligand

The low-energy electronic absorptions can be assigned as MMCT-type transitions from the observation that the NIR

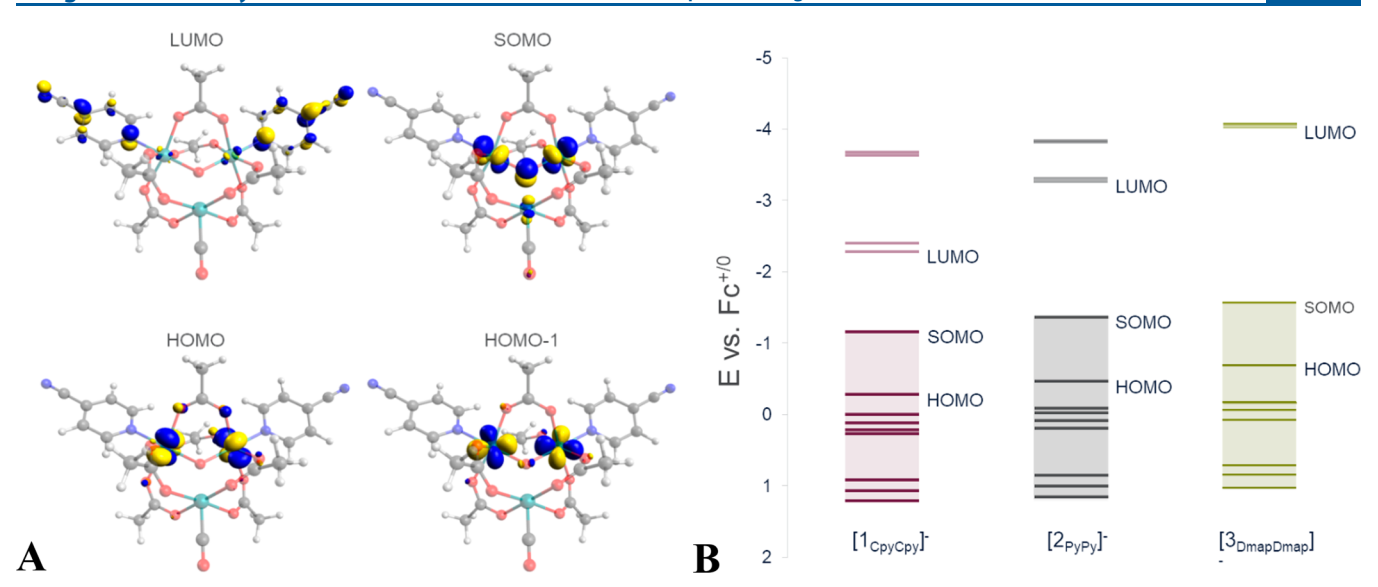


Figure 4. (A) Computed molecular orbitals of [1CpyCpy]⁻, calculated at the uB3LYP level with a B3DJ dispersion correction, showing the three highest energy occupied orbitals (SOMO, HOMO, and HOMO-1) and the lowest energy unoccupied orbital (LUMO). (B) Quasi-restricted molecular orbital (QRO) energy levels (experimentally normalized vs Fc+/0) for the three symmetrically substituted ruthenium molecules, with the 9 highest energy occupied orbitals darkened and shaded up to the energy level of the half-occupied SOMO.

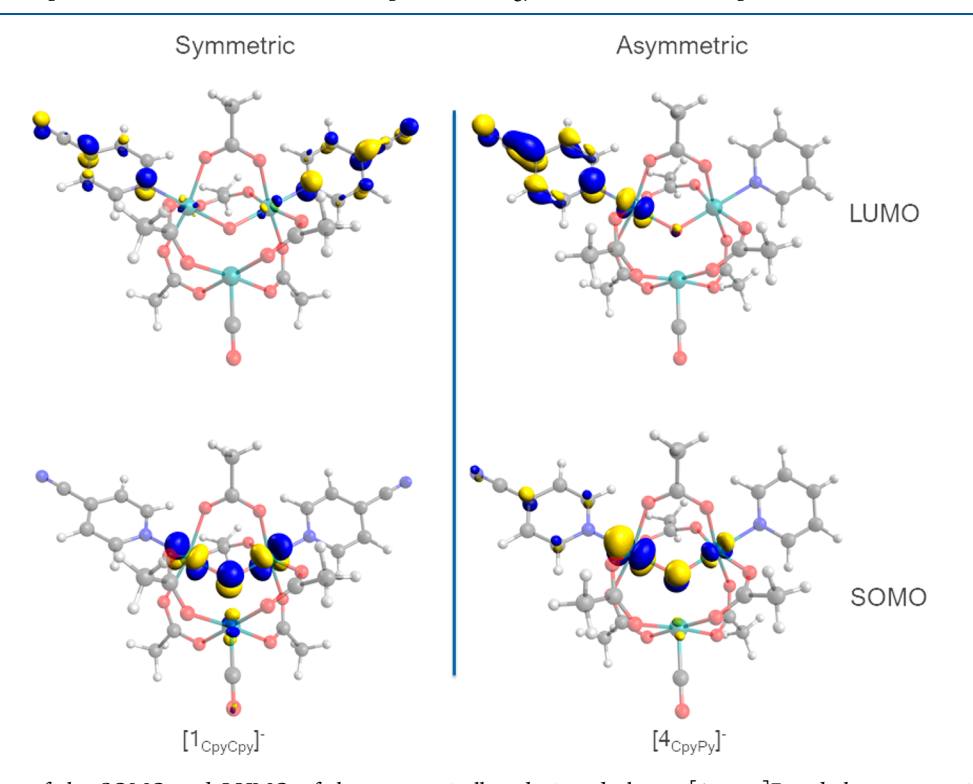


Figure 5. Comparison of the SOMO and LUMO of the symmetrically substituted cluster $[1_{CpyCpy}]^-$ and the asymmetric cluster $[4_{CpyPy}]^-$, displaying the differences in the composition of the orbitals with increasing electron-donor mismatch between the pyridine ligands.

feature does not shift substantially with different ligands and from the mixed-valent nature of the anionic clusters. There is an available transition from the HOMO and the SOMO, with an orbital energy gap at around 7000–8000 cm $^{-1}$ based on the DFT results. While this is slightly lower than the experimentally observed absorptions in all molecules, it does fall within 1200 cm $^{-1}$ of the deconvoluted peak center for all systems studied. The second, higher-energy absorption observed in the NIR ($\lambda_{\rm max} \sim 9500~{\rm cm}^{-1})$ is tentatively assigned as a transition between the second highest fully occupied orbital (HOMO–1) and the SOMO. Across the

series of homoleptic clusters, $[1_{CpyCpy}]^-$, $[2_{PyPy}]^-$, and $[3_{DmapDmap}]^-$, the disappearance of the high-energy MMCT feature coincides with the HOMO and SOMO increasing in energy relative to the rest of the occupied orbitals. The loss of intensity corresponding to a divergence in energy levels could suggest vibronic coupling is responsible for the appearance of this feature and could be of interest for more elaborate computational investigation of these molecules' behavior.

A close examination of the electronic structure of an individual cluster reveals how the mixed-valency manifests itself in the orbital energies. In $[\mathbf{1}_{CpyCpy}]^-$, we observe that the

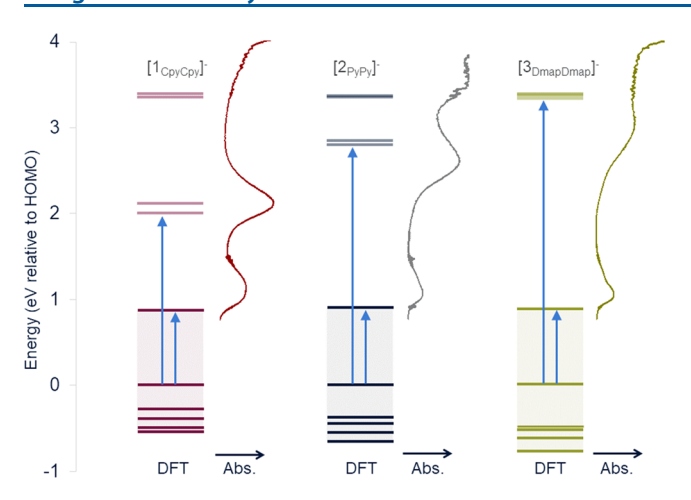


Figure 6. Energy levels of the three symmetrically substituted ruthenium clusters compared with their observed absorbances graphed with the units of energy on the vertical axis centered at the HOMO, with yellow arrows indicating attributed vertical transitions.

d orbitals of the two chemically equivalent ruthenium centers display strong electronic coupling between them as symmetric and antisymmetric combinations of nonbonding d orbitals occur. The degree of energetic splitting between these sets indicates the extent of the coupling for a specific orbital symmetry. The occupied d orbitals with π symmetry across the bridging oxide show the strongest energetic splitting. In contrast, the d orbitals completely residing in the plane of the trinuclear core show essentially no energetic splitting and behave almost as a degenerate set. The d orbitals completely in the plane of the Ru-OAc bonds experience an intermediate degree of energetic splitting between these two extremes. A typical description of this type of mixed-valent system is limited to two parameters, a reorganization energy (λ) and an electronic coupling factor (H_{ab}) . The description provided here expands upon this idea by specifying which orbitals facilitate the electronic coupling and which orbitals remain largely nonparticipatory.

The historical difficulty encountered in describing inorganic mixed-valent molecules with DFT has provided a substantial roadblock to thoroughly describe the electronic structure of these systems. While Marcus-Hush theory provides a framework with which to describe molecules with two interacting electronic states, it does not give a particularly detailed description of the orbitals being populated or how they interact. The manifestation of coupling in a mixed-valent molecule can be restricted to a single pair of identical orbitals, or it could be spread between several orbitals. Understanding which orbitals contribute to these interactions is useful in designing highly coupled chemical systems that have potential applications in molecular electronics or other electronic materials. Upon obtaining high-quality computational descriptions of these mixed-valent molecules, it becomes possible to reach beyond the description provided by the Marcus-Hush theoretical framework to start exploring how the orbitals in mixed-valent molecules interact to facilitate long-range electronic communication.

ASSOCIATED CONTENT

Supporting Information

The Supporting Information is available free of charge at https://pubs.acs.org/doi/10.1021/acs.inorgchem.0c00881.

Synthetic protocols, optimized molecular geometries, and full UV-vis/NIR spectra for all molecules (PDF)

AUTHOR INFORMATION

Corresponding Author

Clifford P. Kubiak — Department of Chemistry and Biochemistry, University of California, San Diego, San Diego, California 92093, United States; orcid.org/0000-0003-2186-488X; Email: ckubiak@ucsd.edu

Authors

Joseph M. Palasz – Department of Chemistry and Biochemistry, University of California, San Diego, San Diego, California 92093, United States

Tyler M. Porter – Department of Chemistry and Biochemistry, University of California, San Diego, San Diego, California 92093, United States; oorcid.org/0000-0002-2693-2653

Complete contact information is available at: https://pubs.acs.org/10.1021/acs.inorgchem.0c00881

Author Contributions

"These authors contributed equally.

Notes

The authors declare no competing financial interest.

ACKNOWLEDGMENTS

We thank Dr. Jacob Barrett for helpful discussions and assistance with the preparation of this manuscript. We acknowledge Dr. Robert Konecny and the W. M. Keck Foundation for assistance and computational resources. The authors gratefully acknowledge financial support from the NSF, under CHE-1853908.

REFERENCES

- (1) Creutz, C.; Taube, H. A Direct Approach to Measuring the Franck-Condon Barrier to Electron Transfer between Metal Ions. *J. Am. Chem. Soc.* **1969**, *91* (14), 3988–3989.
- (2) Yano, J.; Yachandra, V. Mn4Ca Cluster in Photosynthesis: Where and How Water is Oxidized to Dioxygen. *Chem. Rev.* **2014**, 114 (8), 4175–4205.
- (3) Farrar, J. A.; Neese, F.; Lappalainen, P.; Kroneck, P. M. H.; Saraste, M.; Zumft, W. G.; Thomson, A. J. The Electronic Structure of CuA: A Novel Mixed-Valence Dinuclear Copper Electron-Transfer Center. J. Am. Chem. Soc. 1996, 118 (46), 11501–11514.
- (4) Wilkins, P. C.; Wilkins, R. G. The coordination chemistry of the binuclear iron site in hemerythrin. *Coord. Chem. Rev.* **1987**, 79 (3), 195–214.
- (5) Davydov, R.; Kuprin, S.; Graeslund, A.; Ehrenberg, A. Electron Paramagnetic Resonance Study of the Mixed-Valent Diiron Center in Escherichia coli Ribonucleotide Reductase Produced by Reduction of Radical-Free Protein R2 at 77 K. *J. Am. Chem. Soc.* **1994**, *116* (24), 11120—11128.
- (6) Borovik, A. S.; Murch, B. P.; Que, L.; Papaefthymiou, V.; Munck, E. Models for iron-oxo proteins: a mixed valence iron(II)-iron(III) complex. *J. Am. Chem. Soc.* 1987, 109 (23), 7190–7191.
- (7) Proshlyakov, D. A.; Pressler, M. A.; Babcock, G. T. Dioxygen activation and bond cleavage by mixed-valence cytochrome c oxidase. *Proc. Natl. Acad. Sci. U. S. A.* **1998**, 95 (14), 8020.
- (8) Schneider, B.; Demeshko, S.; Dechert, S.; Meyer, F. A Double-Switching Multistable Fe4 Grid Complex with Stepwise Spin-Crossover and Redox Transitions. *Angew. Chem., Int. Ed.* **2010**, 49 (48), 9274–9277.
- (9) Tong, J.; Demeshko, S.; John, M.; Dechert, S.; Meyer, F. Redox-Induced Single-Molecule Magnetism in Mixed-Valent [2 × 2] Co4 Grid Complexes. *Inorg. Chem.* **2016**, *55* (9), 4362–4372.

- (10) Zhao, Y.; Guo, D.; Liu, Y.; He, C.; Duan, C. A mixed-valence (FeII)2(FeIII)2 square for molecular expression of quantum cellular automata. *Chem. Commun.* **2008**, No. 44, 5725–5727.
- (11) Park, J. G.; Aubrey, M. L.; Oktawiec, J.; Chakarawet, K.; Darago, L. E.; Grandjean, F.; Long, G. J.; Long, J. R. Charge Delocalization and Bulk Electronic Conductivity in the Mixed-Valence Metal—Organic Framework Fe(1,2,3-triazolate)2(BF4)x. J. Am. Chem. Soc. 2018, 140 (27), 8526—8534.
- (12) Xie, L. S.; Sun, L.; Wan, R.; Park, S. S.; DeGayner, J. A.; Hendon, C. H.; Dincă, M. Tunable Mixed-Valence Doping toward Record Electrical Conductivity in a Three-Dimensional Metal—Organic Framework. J. Am. Chem. Soc. 2018, 140 (24), 7411–7414.
- (13) Pickup, P. G.; Murray, R. W. Redox conduction in mixed-valent polymers. J. Am. Chem. Soc. 1983, 105 (14), 4510–4514.
- (14) Robin, M. B.; Day, P. Mixed valence chemistry. A survey and classification. Adv. Inorg. Chem. Radiochem. 1968, 10, 247.
- (15) Hush, N. S. Intervalence-transfer absorption. II. Theoretical considerations and spectroscopic data. *Prog. Inorg. Chem.* **2007**, *8*, 391.
- (16) Renz, M.; Kess, M.; Diedenhofen, M.; Klamt, A.; Kaupp, M. Reliable Quantum Chemical Prediction of the Localized/Delocalized Character of Organic Mixed-Valence Radical Anions. From Continuum Solvent Models to Direct-COSMO-RS. J. Chem. Theory Comput. 2012, 8 (11), 4189–4203.
- (17) Renz, M.; Kaupp, M. Predicting the Localized/Delocalized Character of Mixed-Valence Diquinone Radical Anions. Toward the Right Answer for the Right Reason. *J. Phys. Chem. A* **2012**, *116* (43), 10629–10637.
- (18) Parthey, M.; Gluyas, J. B. G.; Schauer, P. A.; Yufit, D. S.; Howard, J. A. K.; Kaupp, M.; Low, P. J. Refining the Interpretation of Near-Infrared Band Shapes in a Polyynediyl Molecular Wire. *Chem. Eur. J.* **2013**, *19* (30), 9780–9784.
- (19) Parthey, M.; Gluyas, J. B. G.; Fox, M. A.; Low, P. J.; Kaupp, M. Mixed-Valence Ruthenium Complexes Rotating through a Conformational Robin—Day Continuum. *Chem. Eur. J.* **2014**, 20 (23), 6895—6908.
- (20) Parthey, M.; Kaupp, M. Quantum-chemical insights into mixed-valence systems: within and beyond the Robin–Day scheme. *Chem. Soc. Rev.* **2014**, 43 (14), 5067–5088.
- (21) Kaupp, M.; Karton, A.; Bischoff, F. A. [Al2O4]-, a Benchmark Gas-Phase Class II Mixed-Valence Radical Anion for the Evaluation of Quantum-Chemical Methods. *J. Chem. Theory Comput.* **2016**, *12* (8), 3796–3806.
- (22) Maier, T. M.; Bahmann, H.; Arbuznikov, A. V.; Kaupp, M. Validation of local hybrid functionals for TDDFT calculations of electronic excitation energies. *J. Chem. Phys.* **2016**, 144 (7), 074106.
- (23) Gückel, S.; Gluyas, J. B. G.; El-Tarhuni, S.; Sobolev, A. N.; Whiteley, M. W.; Halet, J.-F.; Lapinte, C.; Kaupp, M.; Low, P. J. Iron versus Ruthenium: Clarifying the Electronic Differences between Prototypical Mixed-Valence Organometallic Butadiyndiyl Bridged Molecular Wires. *Organometallics* 2018, 37 (9), 1432–1445.
- (24) Spencer, A.; Wilkinson, G. μ-Oxo-triruthenium carboxylate complexes. *J. Chem. Soc., Dalton Trans.* **1972**, No. 14, 1570–1577.
- (25) Spencer, A.; Wilkinson, G. Reactions of μ 3-oxo-triruthenium carboxylates with π -acid ligands. *J. Chem. Soc., Dalton Trans.* **1974**, No. 8, 786–792.
- (26) Goeltz, J. C.; Hanson, C. J.; Kubiak, C. P. Rates of Electron Self-Exchange Reactions between Oxo-Centered Ruthenium Clusters Are Determined by Orbital Overlap. *Inorg. Chem.* **2009**, *48* (11), 4763–4767.
- (27) Goeltz, J. C.; Kubiak, C. P. Mixed Valency across Hydrogen Bonds. *J. Am. Chem. Soc.* **2010**, *132* (49), 17390–17392.
- (28) Goeltz, J. C.; Benson, E. E.; Kubiak, C. P. Electronic Structural Effects in Self-Exchange Reactions. *J. Phys. Chem. B* **2010**, *114* (45), 14729–14734.
- (29) Ohto, A.; Sasaki, Y.; Ito, T. Mixed-Metal Trinuclear Complexes Containing Two Ruthenium(III) Ions and a Divalent Metal Ion, [Ru2M(.mu.3-O)(.mu.-CH3COO)6(L)3] (M = Mg, Mn, Co, Ni, Zn; L = H2O, Pyridine). *Inorg. Chem.* **1994**, 33 (7), 1245–1246.

- (30) Salsman, J. C.; Kubiak, C. P.; Ito, T. Mixed Valence Isomers. J. Am. Chem. Soc. 2005, 127 (8), 2382–2383.
- (31) Ota, K.-I.; Sasaki, H.; Matsui, T.; Hamaguchi, T.; Yamaguchi, T.; Ito, T.; Kido, H.; Kubiak, C. P. Syntheses and Properties of a Series of Oxo-Centered Triruthenium Complexes and Their Bridged Dimers with Isocyanide Ligands at Terminal and Bridging Positions. *Inorg. Chem.* 1999, 38 (18), 4070–4078.
- (32) Moreira, M. B.; Da Silva, C. F. N.; Pesci, R. B. P.; Deflon, V. M.; Nikolaou, S. Revisiting oxo-centered carbonyl-triruthenium clusters: investigating CO photorelease and some spectroscopic and electrochemical correlations. *Dalton Trans.* **2016**, *45* (42), 16799–16809.
- (33) Zhang, H.-X.; Sasaki, Y.; Zhang, Y.; Ye, S.; Osawa, M.; Abe, M.; Uosaki, K. Synthesis and Properties of the Cyano Complex of Oxo-Centered Triruthenium Core [Ru3(μ 3-O)(μ -CH3COO)6(pyridine)-2(CN)]. *Inorg. Chem.* **2014**, 53 (3), 1288–1294.
- (34) Zhou, W.; Zhang, Y.; Abe, M.; Uosaki, K.; Osawa, M.; Sasaki, Y.; Ye, S. Surface Coordination of Nitric Oxide to a Self-Assembled Monolayer of a Triruthenium Cluster: An in Situ Infrared Spectroscopic Study. *Langmuir* **2008**, 24 (15), 8027–8035.
- (35) Cotton, F. A.; Norman, J. G. Structural characterization of a basic trinuclear ruthenium acetate. *Inorg. Chim. Acta* **1972**, *6*, 411–419.
- (36) Hamaguchi, T.; Nagino, H.; Hoki, K.; Kido, H.; Yamaguchi, T.; Breedlove, B. K.; Ito, T. 14 Step-15 Electron Reversible Redox Behavior of Tetrameric Oligomer of Oxo-Bridged Triruthenium Cluster. *Bull. Chem. Soc. Jpn.* **2005**, 78 (4), 591–598.
- (37) Nakata, K.; Nagasawa, A.; Sasaki, Y.; Ito, T. Redox Properties of a Series of Iron(III) Trinuclear Carboxylates, [Fe3(μ 3-O)(μ -RCO2)-6(L)3]n+. *Chem. Lett.* **1989**, *18* (5), 753–756.
- (38) Baumann, J. A.; Salmon, D. J.; Wilson, S. T.; Meyer, T. J. Anisotropic mixed-valence systems. Dimers of the delocalized clusters [Ru3O(CH3CO2)6(L)3]n+. *Inorg. Chem.* **1979**, *18* (9), 2472–2479.
- (39) Wilson, S. T.; Bondurant, R. F.; Meyer, T. J.; Salmon, D. J. Oxidation state properties of delocalized, ligand-bridged metal complexes. [Ru3O(CH3CO2)6L3]n+ and the pyrazine-bridged, cluster-cluster dimer, [Ru3O(CH3CO2)6(py)2]2pyzm+. J. Am. Chem. Soc. 1975, 97 (8), 2285–2287.
- (40) Brunschwig, B. S.; Creutz, C.; Sutin, N. Optical transitions of symmetrical mixed-valence systems in the Class II–III transition regime. *Chem. Soc. Rev.* **2002**, *31* (3), 168–184.
- (41) Ito, T.; Hamaguchi, T.; Nagino, H.; Yamaguchi, T.; Kido, H.; Zavarine, I. S.; Richmond, T.; Washington, J.; Kubiak, C. P. Electron Transfer on the Infrared Vibrational Time Scale in the Mixed Valence State of 1,4-Pyrazine- and 4,4'-Bipyridine-Bridged Ruthenium Cluster Complexes. J. Am. Chem. Soc. 1999, 121 (19), 4625–4632.
- (42) Yamaguchi, T.; Imai, N.; Ito, T.; Kubiak, C. P. A Strongly Coupled Mixed Valence State Between Ru3 Clusters. Intramolecular Electron Transfer on the Infrared Vibrational Time Scale in a Pyrazine (pz) Bridged Dimer of Triruthenium Clusters, [{Ru3(μ3-O)(μ-CH3CO2)6(CO)(abco)}2(μ-pz)] (abco = 1-azabicyclo[2,2,2]-octane). Bull. Chem. Soc. Ipn. 2000, 73 (5), 1205–1212.
- (43) Porter, T. M.; Canzi, G. C.; Chabolla, S. A.; Kubiak, C. P. Tuning Electron Delocalization and Transfer Rates in Mixed-Valent Ru3O Complexes through "Push-Pull" Effects. *J. Phys. Chem. A* **2016**, *120* (32), 6309–6316.
- (44) Weigend, F. Accurate Coulomb-fitting basis sets for H to Rn. *Phys. Chem. Chem. Phys.* **2006**, 8 (9), 1057–1065.
- (45) Nicklass, A.; Dolg, M.; Stoll, H.; Preuss, H. Ab initio energy-adjusted pseudopotentials for the noble gases Ne through Xe: Calculation of atomic dipole and quadrupole polarizabilities. *J. Chem. Phys.* **1995**, *102* (22), 8942–8952.
- (46) Schäfer, A.; Huber, C.; Ahlrichs, R. Fully optimized contracted Gaussian basis sets of triple zeta valence quality for atoms Li to Kr. *J. Chem. Phys.* **1994**, *100* (8), 5829–5835.
- (47) Schäfer, A.; Horn, H.; Ahlrichs, R. Fully optimized contracted Gaussian basis sets for atoms Li to Kr. J. Chem. Phys. **1992**, 97 (4), 2571–2577.

- (48) Grimme, S.; Antony, J.; Ehrlich, S.; Krieg, H. A consistent and accurate ab initio parametrization of density functional dispersion correction (DFT-D) for the 94 elements H-Pu. *J. Chem. Phys.* **2010**, 132 (15), 154104.
- (49) Grimme, S.; Ehrlich, S.; Goerigk, L. Effect of the damping function in dispersion corrected density functional theory. *J. Comput. Chem.* **2011**, 32 (7), 1456–1465.
- (50) Glover, S. D.; Kubiak, C. P. Persistence of the Three-State Description of Mixed Valency at the Localized-to-Delocalized Transition. *J. Am. Chem. Soc.* **2011**, *133* (22), 8721–8731.